Physica B: Condensed Matter 561 (2019) 164–169

Contents lists available at ScienceDirect

Physica B: Condensed Matter

journal homepage: www.elsevier.com/locate/physb

Interface thermal transport of graphene-based intralayer heterostructures

Sha Li[a,1], Zhi-Xin Guo[b,a,*,1], J.W. Ding[a,**]

[a] Department of Physics and Institute for Nanophysics and Rare-earth Luminescence, Xiangtan University, Xiangtan, 411105, China
[b] Center for Spintronics and Quantum Systems, State Key Laboratory for Mechanical Behavior of Materials, School of Materials Science and Engineering, Xi'an Jiaotong University, Xi'an, Shaanxi, 710049, China

A B S T R A C T

We have studied the effects of atomic mass (AM) and interatomic potential (IP) on the interface thermal transport of graphene-based intralayer heterostructures, composed of graphene (Gr) and graphene-like materials (Gx). We find that the phonon mismatch between Gx and Gr, induced by the variations of both AM and IP, leads to an obvious thermal resistance in such a hybrid heterostructure model device, following some scaling laws. Compared with that of graphene, the Kapitza resistance (R) of the hybrid heterostructure increases linearly (in power law) with the decrease (increase) of AM in Gx, whereas its variation with IP presents a contrary behavior. On the other hand, the effective interface thermal resistivity (r) increases parabolically (exponentially) with decreasing (increasing) AM and IP in Gx. We also find that the thermal rectification ratio can be effectively manipulated by the variation of AM and IP. Finally, we illustrate that the obtained scaling laws can be used to estimate r in real heterostructures. This study is expected to provide an efficient way to evaluate the interface effect on thermal transport, which have potential applications in design of high-performance heterostructure-based nanodevices.

1. Introduction

2D materials have trigged considerable research interests due to their unique properties and potential applications since the beginning of this century [1–8]. Recently, heterostructures based on van der Waals interaction between 2D materials have become one of the leading hot topics in condensed matter physics and materials science [9–14]. Besides the well studied interlayer heterostructures (HS), the intralayer HS of monolayer materials were realized in recent experiments, which have attracted particular attention [15–20]. Such heterostructure materials with magical properties offer an ideal platform to realize man-made characteristics and explore novel physical phenomena rarely observed in nature. As one of the fundamental physical properties, thermal conduction in nanostructures is crucial for the performance of nanodevices. Several recent theoretical studies have explored the thermal transport in HS, and ones observed significant thermal resistance and reflections from the heterointerfaces [21–24]. Combined with the unique electronic properties of HS [15–18], the exploration of the interface effects on thermal transport in such intralayer HS can accelerate their further applications in microelectronics and thermoelectrics.

From the viewpoint of phonon scatterings, three factors are expected to be dominating for the interface thermal transport of HS: (1) the atomic mass (AM) of a monolayer material; (2) the interatomic potential (IP) of a monolayer material; (3) the geometry distortions at the interface. The previous studies were usually focused on the combined effect of above factors for several graphene-based HS [21–24]. The underlying physical mechanism and general rule of interface effects on the thermal transport have not been well explored for such intralayered hybrid HS. Their clarification is not only fundamentally interesting but also crucial to designing the HS-based high-performance nanodevices.

For exploring general physics, usually, people construct some artificial lattice models with simple interatomic potentials such as Fermi-Pasta-Ulam (FPU) chain model [25–28]. For the general physics of the intralayer heat transport in the 2D heterostructures, similarly, a more realistic model is built in present work, based on the graphene (Gr) geometry and the famous Tersoff potential [29]. As is well known, Gr has the most typical 2D geometry, and the Tersoff potential has been widely used in describing interatomic interactions of various 2D materials [30–33]. The main characteristics of various 2D materials are then involved into the present model. This allows us to explore the general physics of 2D materials, just as done in the artificial lattice models of FPU chain model. The results can be used to evaluate effectively the thermal resistance of the real 2D heterostructures.

For the HS of monolayer materials, the geometry distortion at the interface is usually insignificant with little lattice mismatch. Thus we focus our investigation on the factors of AM and IP in a device model of

* Corresponding author. Department of Physics and Institute for Nanophysics and Rare-earth Luminescence, Xiangtan University, Xiangtan, 411105, China.
** Corresponding author. Department of Physics and Institute for Nanophysics and Rare-earth Luminescence, Xiangtan University, Xiangtan, 411105, China.
E-mail addresses: zxguo08@xjtu.edu.cn (Z.-X. Guo), jwding@xtu.edu.cn (J.W. Ding).
[1] These authors contributed equally to this work.

https://doi.org/10.1016/j.physb.2019.02.064
Received 12 September 2018; Received in revised form 21 December 2018; Accepted 28 February 2019
Available online 04 March 2019
0921-4526/

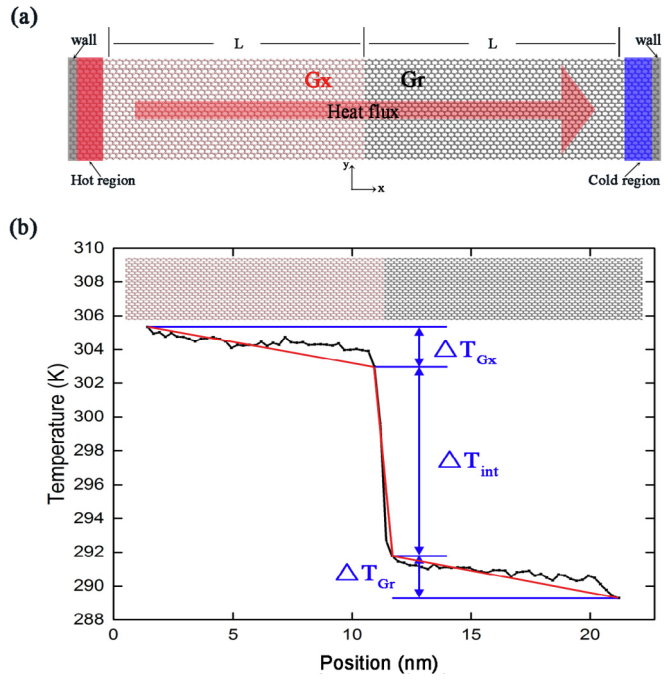

Fig. 1. Geometry of the NEMD simulation for Gx/Gr HS (a) and typical temperature profile along the length direction (b). The heat flux flows from Gx to Gr.

graphene-based intralayer heterostructures, composed of monolayer graphene (Gr) and graphene-like materials with various AM and IP (denoted as Gx). Our study shows that both variation of AM and IP can induce significant thermal resistance and effective thermal resistivity at interface, which can be generally described by scaling laws.

2. Model and methodology

We adopted the nonequilibrium molecular dynamics (NEMD) method [34–36] to investigate the thermal transport property of HS. Fig. 1(a) shows the schematic geometry of Gx/Gr HS, where the heat flux flows from Gx to Gr in x direction. The length of Gx (Gr) was set to be 10 nm, and the width (y direction) in the simulated box was about 5 nm. A periodic boundary condition was applied in y direction, and the fixed boundary condition was used in x direction.

The NEMD simulations were performed using the LAMMPS package [37]. The Tersoff potential was adopted to describe the C-C interatomic interactions in Gr [29]. As for the interatomic interactions in Gx, the same Tersoff potential formula as graphene was adopted, but the parameters for interaction energy were changed by a scaling factor so as to explore the IP effect on the thermal transport. Such a treatment resembles the modification of spring constants in the FPU chain model, which makes sure that other properties are hardly affected such as the graphene geometry and the equilibrium distances between atoms. The interaction between Gx atoms and C atoms are also described by the Tersoff potential formula, where the potential parameters are determined by the mixing rule [30]. Moreover, the velocity Verlet method was used to integrate equations of motion with a fixed time step of 0.5 fs. The system was first fully relaxed in the NVT ensemble at 300 K for 1.25 ns. Then we performed the NEMD simulations, where the outmost two layers of each end of Gx/Gr were fixed, and the adjacent eight layers were coupled to Nosé–Hoover thermostats with temperatures of 310 K and 290 K, respectively. We first performed NEMD simulations for 1.25 ns to make sure that the system gets to the nonequilibrium stationary state, and then performed another 2.5 ns simulation to get the average temperature profile and heat flux.

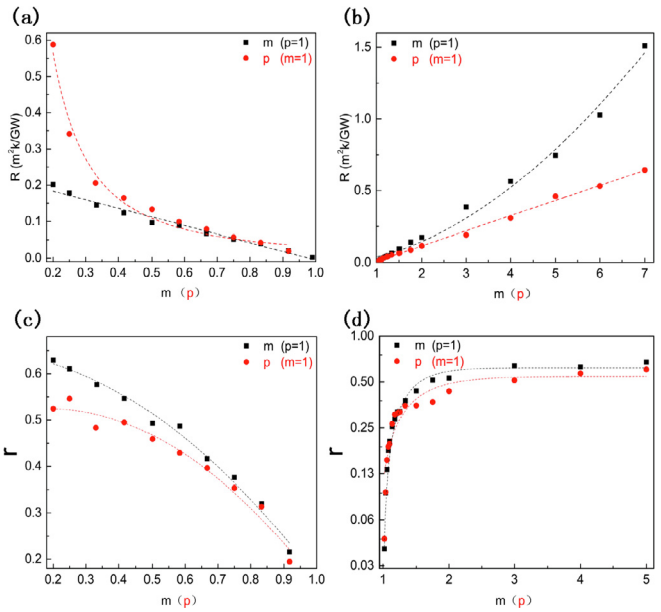

Fig. 2. Calculated m (p) dependence of Kapitza resistance R (a,b) and interface effective thermal resistivity r (c,d) with variation of AM (m) and IP (p) factors in Gx. (a) and (b) correspond to the m (p) dependence of R for m (p) < 1 and m (p) > 1, respectively; (c) and (d) correspond to the m (p) dependence of r for m (p) < 1 and m (p) > 1, respectively. The black squares and red circles represent the variation with m and p, respectively.

3. Numerical results and discussions

For a convenience, we denote m (p) as the ratio of AM (IP) of Gx to that of Gr, which will be the key variables in the following discussions. Also, we define the interface region with two unit cells (0.5 nm), i.e., one unit cell at the Gx side and the other at the Gr side. Fig. 1(b) shows the calculated temperature profile along the length direction of Gx/Gr HS with p = 2 and m = 1. It is seen that a temperature drop ΔT_{int} at the interface is developed, which gives a measurement of the Kapitza resistance $R = \Delta T_{int}/J$, with J being the heat flux [21,38].

To systematically explore the AM and IP effects on the interface thermal resistance, we have considered two cases about Gx: one is for m (p) < 1, and the other is for m (p) > 1. In particular, it is noticed that Gx and Gr are identical at m = 1 and p = 1, where R becomes the smallest. Fig. 2(a) and (b) show the calculated m (p) dependence of R for m (p) < 1 and m (p) > 1, respectively. One can see that in Fig. 2(a), the decrease in AM (m < 1) induces a linear increase of R, scaled by R = 0.230–0.236 m, whereas the increase in AM (m > 1) gives rise to a power-law increase of R in Fig. 2(b), scaled by $R = 0.041\ m^{1.84}$. When the decrease (increase) of IP in Gx from that of Gr, on the other hand, R changes in reverse with the variation of IP, scaled by $R = 0.031p^{-1.795}$ ($R = -0.094 + 0.105p$). This result shows that the decrease of IP and increase of AM have more profound effect on R than the increase of IP and decrease of AM in HS, respectively. The scaling laws obtained above can provide an efficient way to evaluate/manipulate interface thermal resistance.

Since the interface thermal resistance R is determined by two parameters, i.e., ΔT_{int} and J, it is interesting to distinguish the dominating effects on the changes of R with AM and IP. We have further analysed the variation of J and ΔT_{int} with various AM and IP at the interface. It is found that only the variation profile of J is in agreement with that of R, indicating that the change of J is in charge of the variation of R.

In Fig. 2(c) and (d), we further explore the effective interface thermal resistivity (r), defined by $r = \Delta T_{int}/(\Delta T_{Gx} + \Delta T_{int} + \Delta T_{Gr})$, with ΔT_{Gx} and ΔT_{Gr} being the temperature drop in Gx and Gr, respectively [21]. The quantity r represents the ratio of interface thermal resistivity

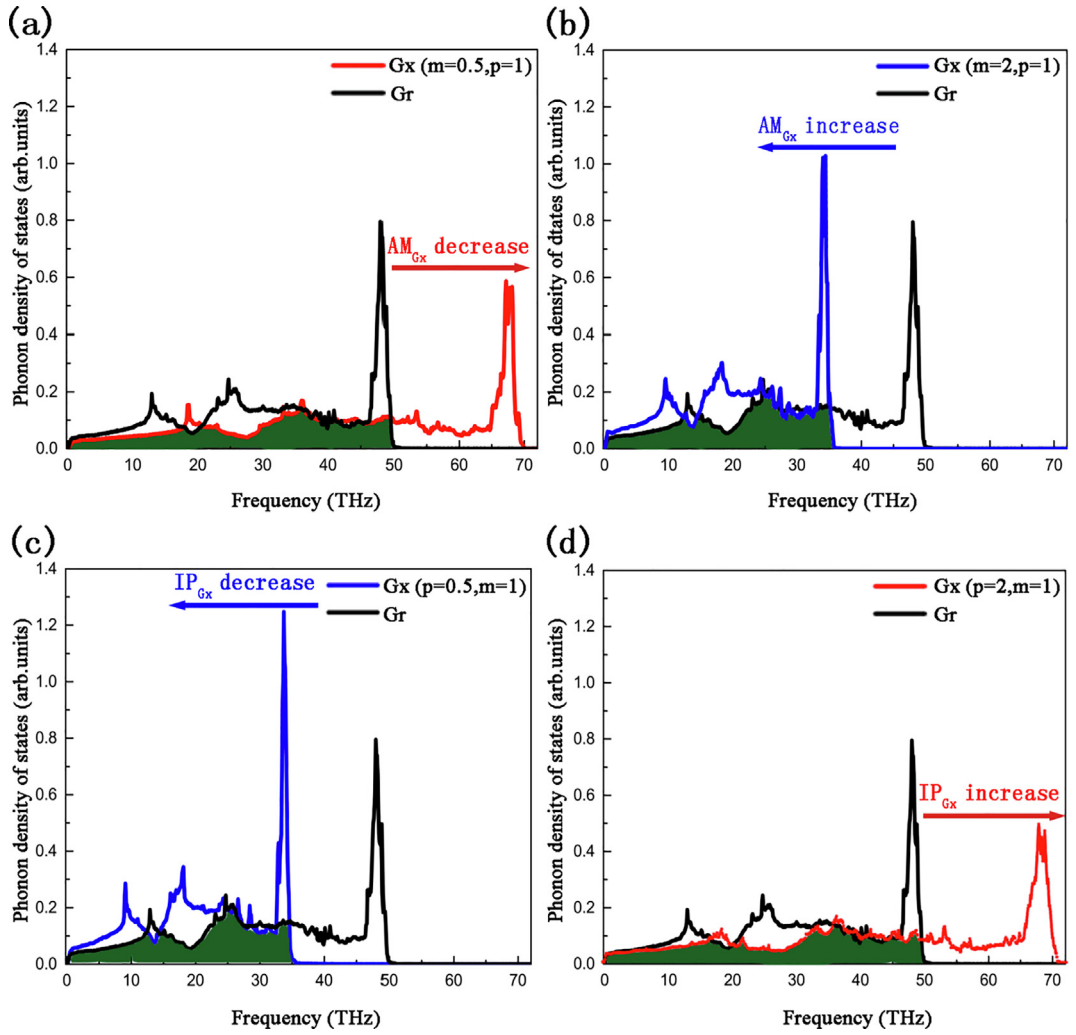

Fig. 3. Phonon density of states (PDOS) of Gx with typical variation of AM and IP, with comparison of Gr. (a) and (b) present the shift of PDOS of Gx with decreasing and increasing AM, respectively. (c) and (d) present the shift of PDOS of Gx with decreasing and increasing IP, respectively.

to the total one in the HS, which is more instinctive in describing the interface effect. In the case of m (p) < 1, one observes from Fig. 2(c) that the AM and IP dependence of r exhibits a parabolic curve, which can be closely approximated by $r = 0.649–0.054m-0.434\,m^2$ under p = 1 and by $r = 0.506 + 0.203p-0.561p^2$ under m = 1. In the case of m (p) > 1, interestingly, it is found from Fig. 2(d) that the variation of r with m (p) follows an exponential curve, which can be well described by $r = 0.619–11.8e^{-m/0.338}$ under p = 1 and by $r = 0.543–3.352e^{-p/0.49}$ under m = 1. In use of such scaling formulae, one can evaluate the efficiency of interface thermal resistance without performing complex computations. From the figures, one can also see that the change of AM induces more significant variation of r than the IP does, showing that adjusting AM is a more efficient way to manipulate r.

To understand the physical mechanism of the interface resistance in HS, we have calculated the phonon density of states (PDOS) of Gx and Gr (Fig. 3). Compared with that of Gr, obvious extension of PDOS to higher frequencies has been observed in Gx with either decreasing AM or increasing IP. On the contrary, increasing AM or decreasing IP induces obvious shrinking of PDOS. From the lattice dynamics theory, one knows that $\omega \propto \sqrt{K/M}$ for the phonon mode of highest frequency (stretch phonon mode), where K and M are the force constant and atomic mass of a material, respectively [39,40]. This allows one to get $\omega_{Gr} \propto \sqrt{K_c/M_c}$, and $\omega_{Gx} \propto \sqrt{K_x/M_x}$, where K_c (K_x) and M_c (M_x) are the force constant and atomic mass of Gr (Gx), respectively. Thus the variation of the highest phonon frequency in Gx can be described as $\omega_{Gx} \propto \sqrt{p/m}$, with $p = K_x/K_c$ and $m = M_x/M_c$. In all the above cases, the variations of both AM and IP lead to the large mismatch of PDOS between Gx and Gr, which in turn result in the large R and r. We have additionally calculated the phonon matching coefficient S in a similar way as reported in Chen's work [41,42]. As shown in Fig. 4(a) and (b), S monotonously decreases with the decrease/increase of AM and IP. This feature is in consistent with the variation of R (r) with AM and IP, showing that the phonon mismatch is responsible for the thermal

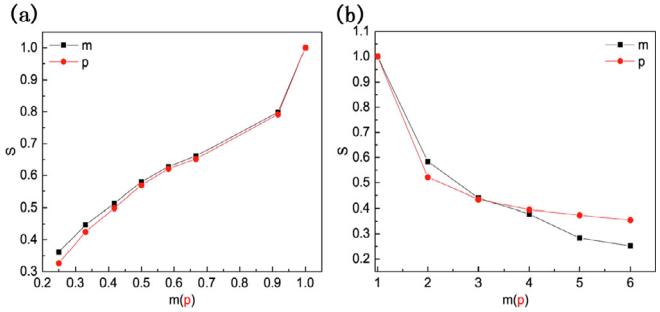

Fig. 4. Calculated phonon matching coefficient S with the decrease (a) and increase (b) of AM (m) and IP (p) factors in Gx. S monotonously decreases with the variation of AM and IP in both (a) and (b). This feature is in consistent with the variation of R (r) with AM and IP, showing that the phonon mismatch is responsible for the thermal resistance at the interface.

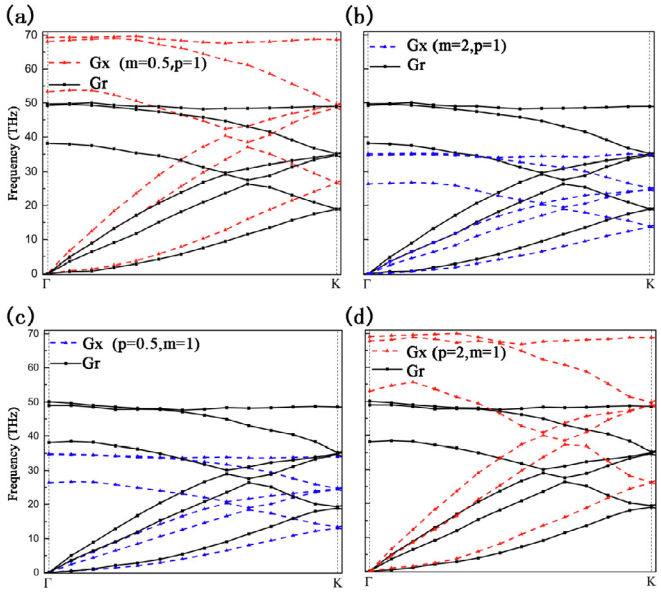

Fig. 5. Phonon dispersions of Gx along the thermal transport direction with typical various AM and IP, with comparison of Gr. (a) and (b) present the phonon dispersions of Gx with decreasing and increasing AM, respectively. (c) and (d) present the phonon dispersions of Gx with decreasing and increasing IP, respectively.

resistance at the interface.

It is noticed that the extension and shrinking of PDOS in Gx correspond to the power-law and linear variations of R, respectively. To have a clear understanding on this phenomenon, we have calculated the phonon dispersions along the thermal transport direction, which correspond to the Γ-K direction in the reciprocal space, for Gx with various AM and IP (Fig. 5). As one can see, decreasing AM or increasing IP not only increases the velocity of three acoustic phonons, but also pushes the optical phonons to higher frequencies (Fig. 5 (a) and 5(d)), which results in the extension of PDOS. Since the acoustic phonons are dominating for the thermal transport in Gr at room temperature [43–47], one can conclude that R is mainly attributed to the variation of acoustic phonons in Gx in this case. On the other hand, increasing AM or decreasing IP have effect of decreasing the velocity of acoustic phonons and pushing the optical phonons to lower frequencies (Fig. 5 (b) and 5(c)), which results in the shrinking of PDOS. The downshifted optical phonons can also be excited due to their lower frequencies, which would effectively interact with the acoustic phonons in Gx via the phonon-phonon scatterings, leading to a decrease of the acoustic phonons transporting across the interface. Thus the downshifted optical phonons are also expected to contribute to R.

As shown in Fig. 5(a) and (b), the mismatches of acoustic phonons induced by decreasing AM by half are similar to that by increasing AM by two times. This implies that the different variations of R with decreasing and increasing AM are resulted from the different effects of upshifting and downshifting optical phonons. In the linear variation case, only the mismatches between acoustic phonons contribute to R. Whereas, in the power-law behavior, the optical phonons in Gx are additionally excited in Gx, but they have little contribution to the thermal transport. This is because the optical phonons are hardly coupled to the acoustic phonons, the main thermal carriers in Gr. However, the excitation of optical phonons in Gx reduces the amount of excited acoustic phonons, which are expected to transport through the interface. Therefore, although the mismatches of acoustic phonons are similar, the interface thermal resistances are very different for decreasing and increasing AM. This mechanism also applies to the variation of R with decreasing/increasing IP. In addition, the different behaviors of r with decreasing and increasing AM (IP) are attributed to the combined

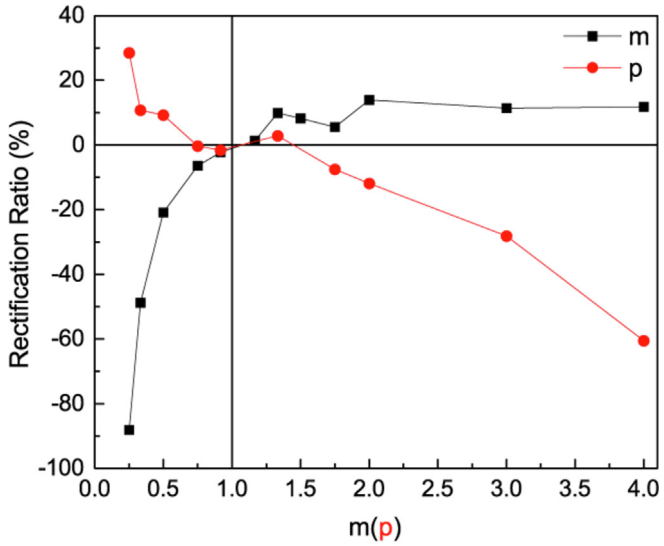

Fig. 6. Calculated thermal rectification ratio (TR) variation with AM (m) and IP (p) factors in Gx at a fixed temperature difference $|\Delta| = 0.067$.

effects from the variations of R and the thermal conductance of Gx.

On the other hand, it is well known that HS structures normally have pronounced thermal rectification effect. We have additionally calculated the thermal rectification ratio (TR) using $TR = \frac{J_+ - J_-}{J_-} \times 100\%$ at a fixed temperature difference $|\Delta|$ with $\Delta = (T_L - T_R)/300$, where J_+ and J_- correspond to $\Delta > 0$ and $\Delta < 0$, respectively [7,46]. As shown in Fig. 6, with a fixed temperature difference $|\Delta| = 0.067$, the decrease in AM ($m < 0$) induces a negative TR, and the increase in AM ($m > 0$) gives rise to a positive TR. Whereas, the change of TR with IP has a contrary behavior. Moreover, the variation of TR is more sensitive to the decrease of IP and AM, where the maximum positive (30%) and negative (−90%) TR values appear with p and m of Gx reaching one quarter, respectively. This result indicates that one can effectively manipulate the thermal rectification via changing AM and IP in the HS.

As an application of our model devices for real systems, we have considered r in Gx/Gr HS, composed of C_{13} randomly doped graphene (considered as Gx) and pure C_{12} graphene (that is, Gr) [48]. Such hybrid structure can be realized through the isotope doping technique. Fig. 7(a) shows NEMD calculated C_{13} doping concentration dependence of r (solid dots), which increases monotonically to 0.13 with the doping concentration increasing to 90%. We have also evaluated r form the above exponential formula ($r = 0.619–11.8e^{-m/0.338}$) in use of the average AM in Gx, which depends only on the doping concentration (open dots). Here m is the ratio of average atomic mass of Gx to that of Gr. For example, we adopted m = 12.5/12 for a 50% doping of C_{13}. It is found that the exponential formula can qualitatively represent the direct NEMD results. The small diverges can be attributed to the randomly distribution of C_{13} in Gx in NEMD calculation, which was considered to be evenly distributed on each atom in the exponential formula.

We have also considered another real case of HS, composed of h-BN and Gr monolayers (h-BN/Gr, Fig. 7(b)) [22,24]. In the ENMD simulation, the Tersoff potential for B-N-C was used to describe the atomic interactions for B-N, B-C, and C-C [30]. The calculated results show that the effective interface thermal resistance of h-BN/Gr is r = 0.475. On the other hand, the value of r can be also evaluated in use of our simulated laws for the system, the first step of which is to evaluate m and p for h-BN. It is noted that there are many phonon modes in the h-BN determined by the AM, IP, as well as the geometry structure. However, the difference between the highest phonon frequencies (stretch phonon mode) of h-BN and Gr are mainly induced by the different AM and IP of the two structures. As discussed above, the ratio (h_{ra}) between the

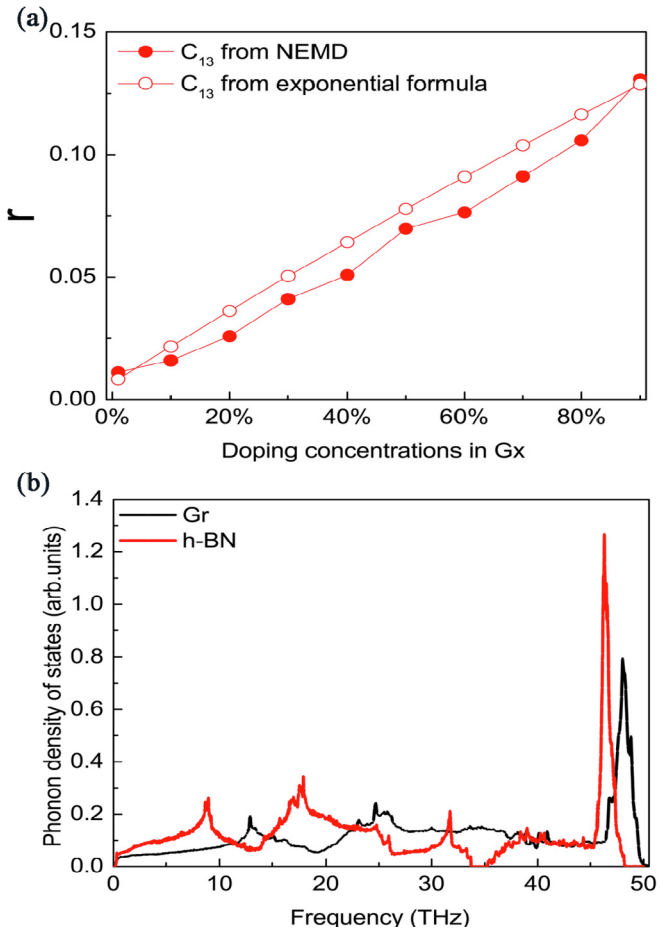

Fig. 7. (a) r variation with C_{13} doping concentration in Gx. The solid and open circles represent the results from direct NEMD calculations and our obtained scaling formula, respectively. (b) Calculated PDOS of h-BN and Gr. The peak of the highest phonon frequency locates at about 46 THz and 48 THz for h-BN and Gr, respectively.

highest frequencies of h-BN and Gr approximatively obtained to be $h_{ra} \approx \sqrt{K_{BN}/M_{BN}}/\sqrt{K_c/M_c}$, where K_{BN} (M_{BN}) and K_c (M_c) are the force constants (average atomic masses) of h-BN and Gr, respectively. Considering that Gx and Gr have the same IP formula, we can have $h_{ra} \approx \sqrt{p/m}$. With $m \approx \sqrt{M_{BN}/M_c} = 1.042$ ($M_{BN} = 12.5$ relative atomic mass) and the value of h_{ra} obtained from the numerical phonon structure calculations, we can get the value of p for h-BN as a result. As indicated by the PDOS in Fig. 7 (b), the highest phonon frequencies of h-BN and Gr are about 46 THz and 48 THz, respectively. Thus one can get $p \approx 0.842$ for h-BN in the HS, which contributes 0.279 to r according to the obtained parabolic rule ($r = 0.506 + 0.203p\text{-}0.561p^2$). On the other hand, the effect of AM on r can be evaluated with m = 1.042, which contributes additional 0.08 to r according to the obtained exponential rule ($r = 0.619\text{–}11.8e^{-m/0.338}$). Therefore, one can get a rough evaluation of r = 0.36 from the model calculations, which is close to the direct NEMD result (r = 0.475).

Additionally, we discuss the interface thermal resistance in another typical HS structure, MoS_2/Gr, where the NEMD simulations predicted $R = 2.5\,km^2/GW$ [49]. The MoS_2/Gr HS is more complex than the Gx/Gr HS owing to the complex MoS_2 geometry. This feature induces significant geometry distortions at the interface which has not been considered in this work. Nevertheless, we can roughly estimate the interface thermal resistance contributed by the mismatch of AM and IP in the MoS_2/Gr HS. According to the atomic mass of Mo, S and C, we can get m = 4.4, corresponding to R = 0.6. Additionally, according to $\omega_{MoS2}/\omega_{Gr} \approx \sqrt{p/m}$ where ω_{MoS2} and ω_{Gr} are the frequencies of the stretch phonon mode of MoS_2 and graphene respectively (their values can be obtained from the phonon structure calculations), we can get $p \approx 0.43$, corresponding to $R = 0.15\,km^2/GW$. This indicates that the thermal resistance from AM and IP is about $0.75\,km^2/GW$ from our obtained numerical laws. This value is in the same order to that in real MoS_2/Gr HS, while it is less than that in the later. The result should be reasonable, since the exclusion of lattice-distortion effect on the thermal resistance in our study is expected to give rise to smaller R.

Finally, we would like to remark that the phonon wave packet simulations can additionally show the dynamical feature of phonon scatterings at the interface. Such calculations had been successfully applied to the MoS_2/Gr HS, and clearly showed how the LA and TA phonons transporting across the interface [49]. The results agree well with the analytical ones obtained from the viewpoint of phonon mismatch for the interface phonon transport. Here the phonon wave packet scattering in Gx/Gr HS is expected to have similar features as that in the MoS_2/Gr HS, i.e., the LA mode has more significant contribution to the thermal transmission, and the low-energy phonons are more efficiently transported across the interface, which are to be confirmed in the feature investigations.

4. Conclusions

In summary, by using the NEMD simulations, we have investigated the effects of atomic mass and interatomic potential on the interface thermal resistance R and effective thermal resistivity r of intralayer heterostructures, via a Gx/Gr device model. We have found that both the variation of AM and IP in Gx can induce large R and r, following scaling laws. Especially, it is found that r increases parabolically (exponentially) with decrease (increase) of AM and IP. The underlying mechanism has been explored from viewpoint of phonon spectra variations, induced by the change of AM and IP, which affects the excited phonons for the heat transfer across the interface. We have also found that the thermal rectification ratio can be effectively manipulated by the variation of AM and IP. Finally, we have illustrated that the obtained scaling laws can be used to evaluate r in real heterostructures. Although the interatomic potentials in an actual 2D heterostructure may have some variations from the Tersoff type, one can always estimate the phonon mismatch from the ratio of atomic mass and strength of interatomic interactions between the two 2D materials. Therefore, we believe that our obtained scaling laws have the general physical meaning, and can be applicable in various actual 2D heterostructures.

Acknowledgment

This work was supported by NSFC (No. 11374245) and the Science Fund for Distinguished Young Scholars of Hunan Province (No. 2018JJ1022).

References

[1] A.K. Geim, Science 324 (2009) 1530.
[2] A.A. Balandin, S. Ghosh, W. Bao, I. Calizo, D. Teweldebrhan, F. Miao, C.N. Lau, Nano Lett. 8 (2008) 902.
[3] A. Gupta, T. Sakthivel, S. Seal, Prog. Mater. Sci. 73 (2015) 44.
[4] K. Novoselov, A. Mishchenko, A. Carvalho, A.C. Neto, Science 353 (2016) 9439.
[5] J. Zhao, H. Liu, Z. Yu, R. Quhe, S. Zhou, Y. Wang, C.C. Liu, H. Zhong, N. Han, J. Lu, Y. Yao, K. Wu, Prog. Mater. Sci. 83 (2016) 24.
[6] G.F. Xie, Z.F. Ju, K.K. Zhou, X.L. Wei, Z.X. Guo, Y.Q. Cai, G. Zhang, npj Comput. Mater. 4 (2018) 21.
[7] G.F. Xie, D. Ding, G. Zhang, Adv. Phys. X 3 (2018) 1480417.
[8] P. Li, X. Li, W. Zhao, H. Chen, M.X. Chen, Z.X. Guo, J. Feng, X.G. Gong, A.H. MacDonald, Nano Lett. 17 (2017) 6195.
[9] L. Britnell, R. Gorbachev, R. Jalil, B. Belle, F. Schedin, A. Mishchenko, T. Georgiou, M. Katsnelson, L. Eaves, S. Morozov, Science 335 (2012) 947.
[10] A.K. Geim, I.V. Grigorieva, Nature 499 (2013) 419.
[11] B. Liu, J.A. Baimova, C.D. Reddy, A.W.-K. Law, S.V. Dmitriev, H. Wu, K. Zhou, ACS Appl. Mater. Interfaces 6 (2014) 18180.
[12] J. Zhang, Y. Hong, Y. Yue, J. Appl. Phys. 117 (2015) 134307.
[13] N.B. Le, T.D. Huan, L.M. Woods, ACS Appl. Mater. Interfaces 8 (2016) 6286.

[14] Y. Chen, Y. Zhang, K. Cai, J. Jiang, J.-C. Zheng, J. Zhao, N. Wei, Carbon 117 (2017) 399.
[15] G. Fiori, A. Betti, S. Bruzzone, G. Iannaccone, ACS Nano 6 (2012) 2642.
[16] Z. Liu, L. Ma, G. Shi, W. Zhou, Y. Gong, S. Lei, X. Yang, J. Zhang, J. Yu, K.P. Hackenberg, Nat. Nanotechnol. 8 (2013) 119.
[17] C. Huang, S. Wu, A.M. Sanchez, J.J. Peters, R. Beanland, J.S. Ross, P. Rivera, W. Yao, D.H. Cobden, X. Xu, Nat. Mater. 13 (2014) 1096.
[18] Z. Zhang, P. Chen, X. Duan, K. Zang, J. Luo, X. Duan, Science 357 (2017) 788.
[19] K.C. Chiu, K.H. Huang, C.A. Chen, Y.Y. Lai, X.Q. Zhang, E.C. Lin, M.H. Chuang, J.M. Wu, Y.H. Lee, Adv. Mater. 30 (2018) 1704796.
[20] Q. Zeng, Z. Liu, Adv. Electron. Mater. 4 (2018) 1700335.
[21] B. Liu, J.A. Baimova, C.D. Reddy, S.V. Dmitriev, W.K. Law, X.Q. Feng, K. Zhou, Carbon 79 (2014) 236.
[22] X.K. Chen, Z.X. Xie, W.-X. Zhou, L.M. Tang, K.-Q. Chen, Carbon 100 (2016) 492.
[23] Y. Li, A. Wei, D. Datta, Carbon 113 (2017) 274.
[24] X. Liu, G. Zhang, Y.-W. Zhang, Nano Lett. 16 (2016) 4954.
[25] S. Lepri, R. Livi, A. Politi, Phys. Rep. 377 (2003) 1.
[26] B. Li, L. Wang, G. Casati, Phys. Rev. Lett. 93 (2004) 184301.
[27] J. Lan, B. Li, Phys. Rev. B 74 (2006) 214305.
[28] Z.X. Guo, D. Zhang, X.G. Gong, Phys. Rev. B 84 (2011) 075470.
[29] J. Tersoff, Phys. Rev. B 39 (1989) 5566.
[30] A. Kınacı, J.B. Haskins, C. Sevik, T. Çağın, Phys. Rev. B 86 (2012) 115410.
[31] J.W. Jiang, Nanotechnology 26 (2015) 315706.
[32] M. Hu, X. Zhang, D. Poulikakos, Phys. Rev. B 87 (2013) 195417.
[33] C. Chen, Y. She, H. Xiao, J. Ding, J. Cao, Z.X. Guo, J. Phys. Condens. Matter 28 (2016) 145003.
[34] Z.X. Guo, D. Zhang, X.G. Gong, Appl. Phys. Lett. 95 (2009) 163103.
[35] Z.X. Guo, J. Ding, X.G. Gong, Phys. Rev. B 85 (2012) 235429.
[36] Y. Wang, K. Zhang, G. Xie, Appl. Surf. Sci. 360 (2016) 107.
[37] S. Plimpton, J. Comput. Phys. 117 (1995) 1.
[38] G.L. Pollack, Rev. Mod. Phys. 41 (1969) 48.
[39] M. Born, K. Huang, Dynamics Theory of Crystal Lattices, Oxford University Press, 1954.
[40] V.N. Popov, V.E. Van Doren, Phys. Rev. B 61 (2000) 3078.
[41] X.K. Chen, J. Liu, Z.-H. Peng, D. Du, K.-Q. Chen, Appl. Phys. Lett. 110 (2017) 091907.
[42] X.K. Chen, Z.-X. Xie, W.-X. Zhou, L.-M. Tang, K.-Q. Chen, Appl. Phys. Lett. 109 (2016) 023101.
[43] D. Nika, E. Pokatilov, A. Askerov, A. Balandin, Phys. Rev. B 79 (2009) 155413.
[44] L. Lindsay, D. Broido, N. Mingo, Phys. Rev. B 82 (2010) 115427.
[45] S. Ghosh, W. Bao, D.L. Nika, S. Subrina, E.P. Pokatilov, C.N. Lau, A.A. Balandin, Nat. Mater. 9 (2010) 555.
[46] Y.-Y. Liu, W.-X. Zhou, L.-M. Tang, K.-Q. Chen, Appl. Phys. Lett. 105 (2014) 203111.
[47] Y. Shen, G. Xie, X. Wei, K. Zhang, M. Tang, J. Zhong, G. Zhang, Y.-W. Zhang, J. Appl. Phys. 115 (2014) 063507.
[48] Q.-X. Pei, Y.-W. Zhang, Z.-D. Sha, V.B. Shenoy, Appl. Phys. Lett. 100 (2012) 101901.
[49] X. Liu, J. Gao, G. Zhang, Y.-W. Zhang, Nano Research 10 (2017) 2944.